BIOMICROFLUIDICS **10**, 034114 (2016)

Multiplexed immunosensing and kinetics monitoring in nanofluidic devices with highly enhanced target capture efficiency

Yii-Lih Lin,[1,2,3] Yen-Jun Huang,[3,4] Pattamon Teerapanich,[5,6] Thierry Leïchlé,[5,6] and Chia-Fu Chou[2,3,a)]
[1]*Department of Chemistry, National Taiwan University, Taipei, Taiwan*
[2]*Nano Science and Technology Program, Taiwan International Graduate Program, Academia Sinica and National Taiwan University, Taipei, Taiwan*
[3]*Institute of Physics, Academia Sinica, Taipei, Taiwan*
[4]*Department of Physics, National Taiwan University, Taipei, Taiwan*
[5]*LAAS-CNRS, 7 Avenue du Colonel Roche, F-31077 Toulouse, France*
[6]*Université de Toulouse, F-31077 Toulouse, France*

(Received 12 May 2016; accepted 16 May 2016; published online 7 June 2016)

Nanofluidic devices promise high reaction efficiency and fast kinetic responses due to the spatial constriction of transported biomolecules with confined molecular diffusion. However, parallel detection of multiple biomolecules, particularly proteins, in highly confined space remains challenging. This study integrates extended nanofluidics with embedded protein microarray to achieve multiplexed real-time biosensing and kinetics monitoring. Implementation of embedded standard-sized antibody microarray is attained by epoxy-silane surface modification and a room-temperature low-aspect-ratio bonding technique. An effective sample transport is achieved by electrokinetic pumping via electroosmotic flow. Through the nanoslit-based spatial confinement, the antigen-antibody binding reaction is enhanced with ∼100% efficiency and may be directly observed with fluorescence microscopy without the requirement of intermediate washing steps. The image-based data provide numerous spatially distributed reaction kinetic curves and are collectively modeled using a simple one-dimensional convection-reaction model. This study represents an integrated nanofluidic solution for real-time multiplexed immunosensing and kinetics monitoring, starting from device fabrication, protein immobilization, device bonding, sample transport, to data analysis at Péclet number less than 1. *Published by AIP Publishing.* [http://dx.doi.org/10.1063/1.4953140]

INTRODUCTION

Antibody-based array technologies have been widely applied as a powerful proteomic methodology, which shows great potential to simultaneously determine the abundance of multiple biomarkers,[1–4] and for biomarker discoveries for various diseases such as asthma,[5] Down syndrome,[6] pancreatitis,[7] etc. Integration of the antibody arrays with microfluidic technology brings together the advantages of biomolecule specificity and the power to process minute sample volumes.[8] Reducing the dimensions of fluidic channels down to the nanoscale promises high reaction efficiency and fast kinetic responses by confining the diffusion distance that target molecules must travel before being captured by surface immobilized sensors, with an added advantage of much reduced sample volume.[9–12] In nanofluidic channels, high efficiency of single type of immunoreactions has been demonstrated.[12] However, the implementation of a panel of immunoassays for multiplexed biomarker detection remains a challenging task.[13] One of the major technical hurdles lies in the chip bonding chemistries, which mostly involve heat

[a)]Author to whom correspondence should be addressed. Electronic mail: cfchou@phys.sinica.edu.tw

treatment, thereby inducing irreversible damage to any pre-immobilized biomolecules. To avoid this issue, sensor immobilization must be performed after bonding; yet, this presents another challenge: once the chips are encapsulated, multiplexed immobilization inside the channels becomes a technical hurdle,[14] which may involve multiple runs of reagent exchanges and washing steps, thus rendering the devices impractical for real-world applications. Though several strategies have been attempted to implement multiple immunoassays in the encapsulated microfluidic channels, including the use of photo-crosslinking chemicals to retain antibodies locally[12] and laminar flow for parallel immobilization,[15] none of these have been applied to encapsulated nanofluidic devices.

To overcome these issues, we developed a strategy of using low-aspect-ratio ($\sim 5 \times 10^{-4}$, height/width) nanofluidic slits (nanoslits) with 1-mm width to allow the multiplexed immobilization of the entire antibody microarray panel using a commercially available robotic microarray spotter. The chosen slit height of 500 nm is comparable to the diffusion distance of protein at the millisecond scale ($x = \sqrt{2Dt} \sim 0.4\,\mu$m as $t = 1$ ms), which brings the antigens extremely close to the surface-immobilized antibodies for enhanced binding reaction. To achieve this goal, we developed a *room-temperature* bonding technique involving a thin layer of conformable polysilsesquioxane (PSQ) polymer.[16,17] Since heating is not required during the bonding process, antibody immobilization was performed *open-top prior to* the chip sealing of forming nanofluidic devices. Though there are reported modifications of nanofluidic devices with single type of molecules such as silane,[11] biotin,[9] streptavidin,[18] and oligonucleotides,[17] to our knowledge, this work represents the first attempt to pattern multiplex antibodies as protein microarrays inside spatially confined nanoslits while capable of monitoring spatially distributed antigen binding kinetics in real time using pixelated imaging data, in contrast to most biosensors, where a single averaged response curve is obtained. Here, electroosmotic flow was used as the pumping mechanism for sample transport to overcome the deficiency of pressure-driven flow in the high flow resistance regimes of the extended nanofluidic systems.[19,20] We further developed a simple one-dimensional convection-reaction model enabling the extraction of either the kinetic constants or the target concentration and surface probe density in a given experiment.

EXPERIMENTAL

Device fabrication: Figure 1 displays a schematic of the chip fabrication and antibody immobilization procedure. To create the extended nanofluidic channels, fused silica chips were first patterned with nanoslits using standard photolithographic processes (Microposit S1813 photoresist and MF-319 developer, Shipley, MA) and etched using ICP (RIE-10iP, Samco, Japan). Nanoslits were 1 cm long, 1 mm wide, and 500 nm deep. After defining the sample loading holes using a sand blaster, the chips were cleaned with piranha solution (H_2O_2/H_2SO_4, 1:3 v/v), rinsed extensively with distilled water, and dried by nitrogen purging. The chips were then placed in a Teflon beaker containing 1% (v/v) (3-glycidyloxypropyl)trimethoxysilane (Sigma-Aldrich, St. Louis, MO) in methanol for a 10-min reaction. While several articles have summarized the surface chemistries for antibody immobilization,[21–24] the generic protocol involves soaking the chips with silane solution for multiple hours or even overnight to maximize the epoxy density which leaves little hydroxyl group on the SiO_2 surface. The transient 10-min reaction creates a moderate silane surface density, which not only provides covalent linkage but also creates proper surface hydrophilicity for antibody spot diameters being controlled within 90 to 120 μm. Furthermore, the transient surface modification leaves abundant surface hydroxyl groups, which are essential for silanol condensation reactions between polysilsesquioxane (PSQ) and SiO_2 surfaces in the following chip bonding step.[17]

After surface modification, the chips were precisely located on a robotic arrayer (CapitalBio, Beijing, China) and spotted with the capturing antibody (1.2 mg/ml) in 0.5× PBS (5 mM sodium phosphate, 125 mM NaCl, pH 7.4) solutions. The components of the antibody solutions play a very important role in the microspot morphology,[25,26] in that sufficient antibody concentration is critical to the homogeneity of the fluorescence on the microspot. A concentration lower than this level frequently leads to severe edge effects, in which only the

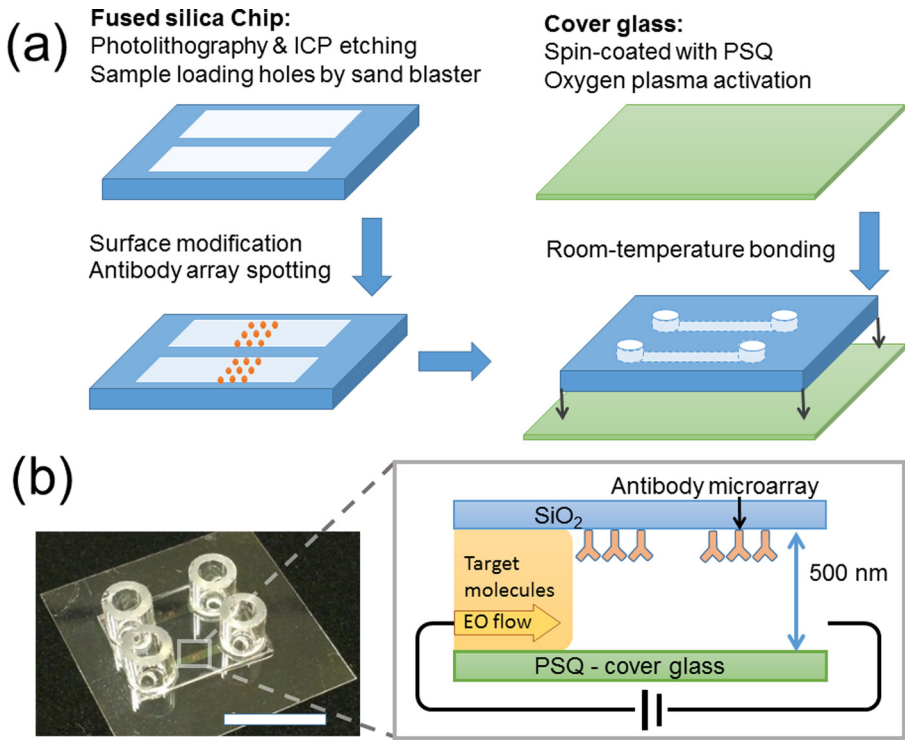

FIG. 1. (a) Schematic of the fabrication procedures of extended nanoslit-based antibody microarray. (b) Photographic image of the fabricated device installed with fused silica tubes as sample reservoirs and a zoomed-in schematic of target molecules flowing in by electroosmotic flow and diffusing through the antibody microarray in the extended nanoslit (scale bar = 1 cm).

periphery has significant signal but not the center of the microspot. Moreover, the antibody solutions partially dehydrated after the spotting step would reduce the height of the spotted antibody to be contained within the extended nanoslits without interfering the following bonding step.

After spotting, the chips were further bonded via a room-temperature bonding method to avoid the denaturation of immobilized biomolecules on the chip surface. This method enabled the direct immobilization of antibodies in the desired locations along the nanofluidic channel before the encapsulation process. Using a thin gasket layer of PSQ, the fused silica (Plan Optik AG, Elsoff, Germany) chip and the cover glass (EMS, Hatfield, PA) were sealed directly. Briefly, the PSQ was prepared by mixing Hardsil-AP (Gelest, Morrisville, PA) with xylene in a 1:2 ratio and spin-coated on a pre-cleaned cover glass. The PSQ coated cover glasses were cured at 240 °C to cross-link the PSQ and surface-activated via oxygen plasma (power of 7.16 W, oxygen pressure of 500 mTorr, and reaction duration of 100 s (Harrick Plasma, Ithaca, NY). With this technique, surface activation using oxygen plasma is required only for the PSQ-cover glass surface, not the antibody-nanoslit surface. Therefore, chemical linkers and the spotted antibodies are preserved without being damaged. The bonded chips were then stored at 4 °C overnight to ensure thorough immobilization reaction. Quartz tubes were then attached as the sample/buffer loading reservoirs before observation with a microscope.

Observation of the immunochemical reaction using fluorescence microscopy: Extended nanoslits were first hydrated by adding a PBS buffer, which was then replaced by bovine serum albumin (BSA) (1 mg/ml) solution. Gold electrodes were placed in the reservoirs, and proteins were driven through the nanoslits by electroosmotic flow with a 450 μm/s linear flow rate using a 200 V/cm electric field. Though many surface passivation methods have been applied in the literature to reduce the non-specific adsorption of target molecules, most of which require an extended time (in hours) to incubate fluidic channels with blocking reagents such as polyethylene glycol (PEG).[9] Here, instead of using the commonly practiced pre-blocking methods for

antibody microarray, we used a dynamic passivation method by adding BSA directly to the antigen solution.[27,28] This method circumvents the need for complicated buffer exchange steps. Based on our results, the addition of 1 mg/ml of BSA into the antigen solution would be sufficient for detection level of 0.1 nM of fluorescent proteins in 10 min. Although BSA concentration is fixed throughout the study, the detailed effects of dynamic BSA adsorption and their effects on electroosmotic flow are under study and will be published elsewhere.

A short blocking step was performed by driving the BSA solution through the nanoslits for 1 min, which was sufficient to fill the nanoslits with BSA, and then, the inlet reservoir was filled with 20 μl of fluorescently labeled antigen mixed with BSA solution. Fluorescence images of the labeled antigen binding to the antibody microarray spots were recorded by time-lapse imaging using a 10× objective with a numerical aperture of 0.45 on an Olympus IX71 microscope with an EMCCD (C9100-13, Hamamatsu, Japan) or a Leica DMI6000B with iXon EMCCD (Andor, Belfast, UK). Both microscopes were installed with mechanical shutters to reduce the photobleaching between the exposure periods.

Simulation: We used computer simulation to model the experimental kinetic curves. First, we used COMSOL (COMSOL AB, Stockholm, Sweden) to solve the partial differential equations (PDE) for convection-diffusion-reaction. A two-dimensional model was created to represent the vertical cross-section along the extended nanoslit. The inlet boundary was set to the initial antigen concentration C_0. Three 90-μm regions were set as the surface concentration of the immobilized antibodies B_0. Instead of using a pressure-driven flow, which has a parabolic flow profile, this study used electroosmotic flow, and thus, a plug flow with a constant flow rate was obtained. The model was solved stepwise throughout the reaction duration for the antigen concentration in bulk and the surface concentration of the captured antigen. Further, we developed a simplified one-dimensional model for rapid simulation of the reaction kinetics in the extended nanoslits. In the model, the two-dimensional domain was further simplified into a one-dimensional linear space based on the fact that diffusion is extremely efficient, making the vertical concentration gradient negligible. Briefly, the model defines a linear space with segmented elements to represent the locations along the nanoslit. One end of the linear space was defined as the inlet with C_0, and the other end was defined as the outlet. Three regions along the linear space were defined as B_0^e, the effective initial concentration of the immobilized antibody microspots. The progress of the plug flow was represented by iterations of segmented small steps in time, each step with a small forward movement of C_0 and a short time duration to allow the immunochemical reaction to occur. The antigen concentrations at each step were saved and plotted to present the simulation result. MATLAB (The MathWorks, Inc., Natick, MA) was used for the simulations, and the required computation time relied on the size of the linear space and the number of steps calculated.

RESULTS AND DISCUSSION

Multiplexed immunoassay in an extended nanoslit

In performing multiplex detection using our assay, the immobilization of the antibody microarray is the most critical procedure. First, the specificity of antibodies should be preserved so that the array can capture the target molecules rather than bind non-specifically. Second, the immobilized antibodies should be fixed tightly *in situ* so that they are not flushed away and do not interfere with the downstream microspots. To verify that these requirements are satisfied, a staggered array of capturing antibodies (cAb), goat anti-rabbit IgG, and rabbit anti-goat IgG was immobilized using a robotic arrayer. Two antigens, goat IgG-Alexa Fluor 647 conjugate and rabbit IgG-Alexa Fluor 488 conjugate (200 nM, each), were loaded to reveal the binding specificity of the individual microspots. Images were taken after the array reached a saturated intensity (Fig. 2(a)). The level of the background noise was low, hence without the need of using any washing steps after antigen binding. As shown in Fig. 2(b), the intensity plot indicates that the background level was ∼5% in relative intensity for both the Alexa 488 and Alexa 594 channels, indicating the non-specific adsorption of antigens onto the slit surface was minimal. Moreover, the antibody specificity was well preserved. The binding of labeled antigens

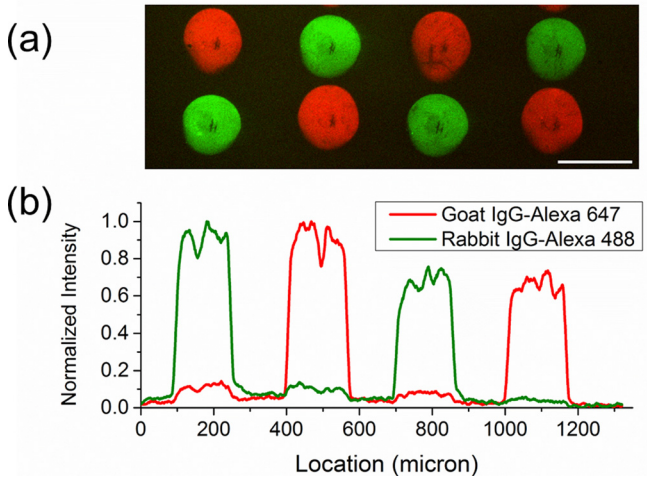

FIG. 2. Fluorescence image and intensity profiles of the antibody microarray in extended nanoslits. (a) Fluorescence images of a 2 × 4 antibody microarray (after 7 min of flowing 200 nM targets). Two sets of antibody microspots were immobilized interlaced (rabbit anti-goat and goat anti-rabbit antibodies) to capture targets of Alexa 488-goat-IgG (green) and Alexa 594-rabbit-IgG (red), respectively. (Scale bar = 200 μm) (b) Line scans along the center of the microspots (from left to right). Intensity values were running averaged by every ten points and normalized to the highest peak value.

onto the non-conjugating microspots was responsible for only ∼5% of the fluorescence intensity increase. These results demonstrate that the immobilized antibodies are capable of differentiating and capturing specific antigens in a multiplex manner.

Immunoreaction kinetics in an extended nanofluidic antibody microarray

To investigate the antibody-antigen binding reaction, we implemented antibody microarrays in extended nanoslits and observed the fluorescence signal when fluorescently labeled antigens bind to the microarrays. The fluidic chips with extended nanoslits were fabricated with three consecutive microspots of identical capturing antibodies (rabbit anti-goat IgG antibody) with a diameter of 93.1 ± 4.1 μm and a center-to-center distance of 200 μm. Corresponding fluorescently labeled antigens (10 nM goat IgG conjugated with DyLight-488) were then introduced with a 450 μm/s flow rate using an applied electric field of 200 V/cm.

Figure 3(a) displays typical representative images after the introduction of the labeled IgG (flux from left to right, multimedia view), with Fig. 3(b) as the reaction schematic. The reaction initiation time was estimated when the target molecules reached the antibody microarrays, and the images before the initiation of the reaction were averaged and subtracted as the background intensity level. The binding reaction of labeled IgG initiates sequentially from the upstream (left) to the downstream (right) microspots. The vast majority of target molecules are captured at the upstream microspots, leaving fewer target molecules for capture at the downstream microspots as indicated by the dark depletion zone representing the high-efficiency capture of target proteins. The sequential onset of the kinetic binding curves (Fig. 3(c)) demonstrates the high efficiency characteristic of the binding reaction in extended nanoslits, as shown by the accumulated binding efficiency, i.e., the ratio of the background subtracted total intensity at the upstream spot (I_1) versus that of the summed intensity of I_1 and the depletion zone of the downstream microspot (#3), I_3, at the fast rising region of the kinetic curves, i.e., $I_1/(I_1 + I_3)$, which is 97.4% at 100 s and 95.2% at 200 s.

Moreover, the low background level is yet another feature; after 600 s of reaction time, while the raw fluorescence intensity count of the first spot increased to a saturated level, the background noise level increased by only 2% compared to the saturation level of the first spot (Fig. 3(c)). The background noise from the solution phase carrying the fluorescently labeled antigen was significantly minimized by the lowered channel height in the extended nanoslit. Therefore, the binding kinetics of the antibody-antigen reaction can be observed real-time,

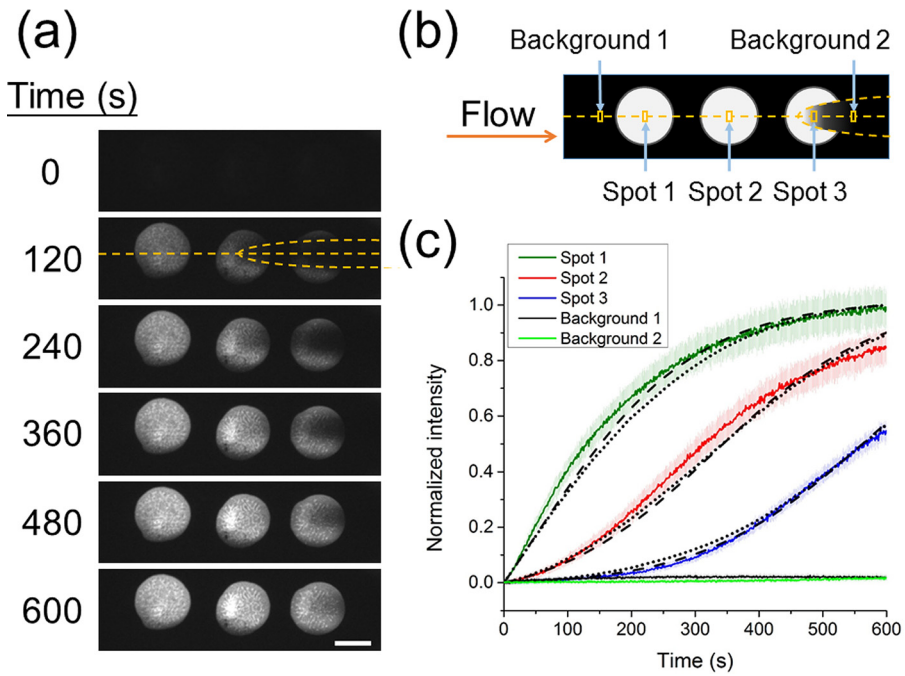

FIG. 3. (a) Real-time imaging of the binding of the 10 nM DyLight 488-conjugated IgG proteins to the immobilized antibody microarray (three identical microspots) in extended nanoslit (flow from left to right). A dark depletion zone representing the high-efficient consumption of target proteins was observed at the downstream microspots. (Scale bar = 100 μm). (b) Schematic of the reaction at t = 360 s. (c) Normalized intensity of the center of the three microspots. All intensities were averaged from an area of 18 × 16 pixels at the center of the corresponding microspots, with the shadowed zones represent standard deviation, and normalized to the intensity of Spot 1 at 600 s. Dashed and dotted lines represent the simulated results using the convection-reaction (CR) model and finite-element methods (FEM), respectively. (Multimedia view) [URL: http://dx.doi.org/10.1063/1.4953140.1]

without the necessity of pausing the sample flux or applying additional washing steps to remove the background fluorescence from non-binding molecules. Moreover, typical microfluidic immunoassays require individual channels and valves to separately introduce the sample and washing solution, while immunoassays in our extended nanoslits do not involve these procedures, thus greatly simplifying the fluidic design.[32,33] In addition, our nanoslit embedding microarray-based platform stands out with real-time sensing and simultaneous monitoring of multiple binding kinetics on multiplexed microarray spots, virtually pixel by pixel, when compared to generic biosensor systems such as quartz crystal microbalance (QCM) and Biacore surface plasmon resonance (SPR) platforms which provide only a single response curve.

To evaluate the response time, three concentrations of target molecules were applied: 0.1, 1, and 10 nM. Intensities in the center of the microspots were averaged (Fig. 4). The time required for the signal to be three-fold higher than the standard deviation of the background was ∼25 s for 10 nM, ∼50 s for 1 nM, and ∼300 s for 0.1 nM. A lower concentration of target yields a slower reaction rate and thus a longer reaction time to acquire a significant signal. However, our device was able to detect fluorescently tagged protein concentrations as low as 0.1 nM within ∼5 min (Fig. 4(b)), which is significantly faster than prior reported works.[9,11] The sensitivity could be further improved via incorporation of surface immobilization techniques such as dendrimer-conjugations[34] and incorporating a carboxymethylated dextran substrate.[35]

Modeling reaction kinetics in extended nanoslits

In this section, we try to model the reaction kinetics by comparing two modeling methods, namely, the finite element method (FEM) and the simplified convection-reaction (CR) model, to experimental data in the hope that it could provide tools to extract parameters such as kinetic

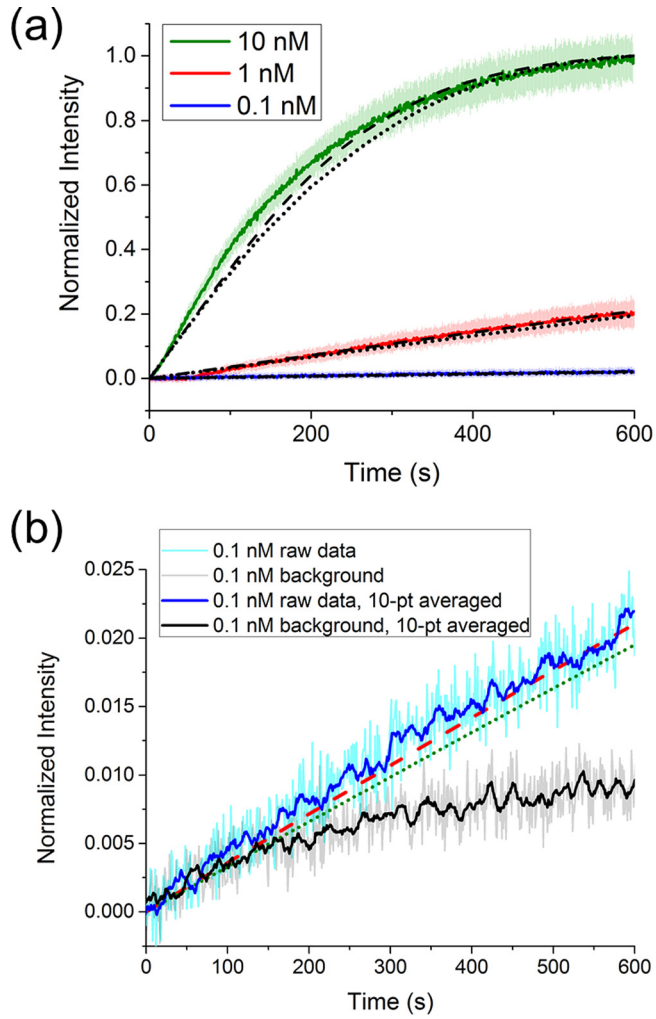

FIG. 4. Comparison of the real-time sensing curves and the simulated results. (a) 0.1, 1, and 10 nM of DyLight 488-conjugated Goat-IgG were used as target proteins. Intensity values were background-subtracted and normalized to the intensity of 10 nM at 600 s. Dashed and dotted lines are simulated results using CR model and FEM, respectively. (b) Expanded view of the 0.1 nM data (blue) and the background (black) are 10-point running averaged. Simulated curves are from CR model (red dashed) and FEM (green dotted).

constants or target concentration and surface probe density in future applications. For typical heterogeneous immunoassays in a microfluidic device, three factors determine the sensor responses: the convection of target molecules toward the antibody microarray, the diffusion of antigens moving along the gradient from the bulk to the surface, and the binding reaction in which target molecules bind to the associated antibodies.[36] Modeling the above convection-diffusion-reaction scenario is typically carried out by solving partial differential equations numerically, using FEM.[29–31,37,38] However, here the slit heights of the extended nanoslits are much smaller than the diffusion distance associated with the target flow time over the sensor microspot ($P_e < 1$, see below), the vertical concentration gradient above the microspots becomes extremely small and thus can be ignored. This leads to a simplified one-dimensional CR model (1D-CR), without the need to solve finite element models and thus simple enough to be implemented with limited computational resources. The 1D-CR model was performed by first creating a 1D space with length L to represent the geometry of the nanoslit, which was divided into discrete elements dL (Fig. 5(a)). To consider the fact that the antibody microspots were confined in an extremely shallow space, we introduced the concept of "effective concentration," which converts the initial surface antibody density B_0 to a volume concentration $B^e = B_0/H$.

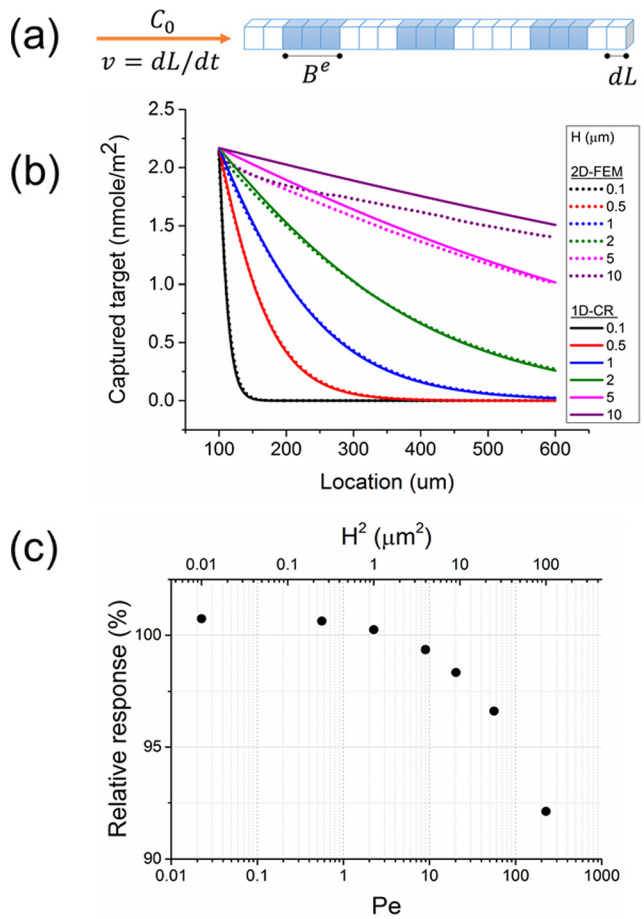

FIG. 5. Direct comparison of the 1D-CR model and 2D-FEM for IgG-anti IgG binding curves. (a) Schematic of the 1D-CR model, where extended nanoslit was represented by grids of unit length dL and microspot locations are assigned B^e as surface antibody density. Reaction begins as target molecules with concentration C_0 moves along the grids with velocity $v = dL/dt$. (b) Comparison of 1D-CR/2D-FEM simulation data with slit height (H) from 0.1 to 10 μm. Surface concentration of captured target represents binding on antibody microspot after 60 s of reaction with 10 nM of target protein. (c) Relative response (1D-CR/2D-FEM) versus the squared slit height (H^2) and Péclet numbers (Pe). Parameters used here are $D = 100\,\mu\text{m}^2/\text{s}$, flow rate $v = 450\,\mu\text{m/s}$, forward reaction rate $k_a = 7.60 \times 10^5\,\text{M}^{-1}\text{s}^{-1}$, and reverse reaction rate $k_d = 5 \times 10^{-4}\text{s}^{-1}$, initial target concentration $C_0 = 10\,\text{nM}$, and initial surface antibody concentration $B_0 = 6\,\text{nmol/m}^2$ (see text).

Thus, for an immobilized antibody spot with a surface concentration of $10^{-8}\,\text{mol/m}^2$, the effective volume concentration B^e would be 20 μM for a channel height of 0.5 μm and would be 10 μM for a 1–μm channel height. The elements representing the location of the antibody microspots were assigned with initial concentration B^e, and the flanking regions were assigned zeroes to indicate that no reaction would happen. Afterward, the target molecules with initial concentration C_0 were introduced to the 1D space with a flow rate v. The forward movement of the target solution was expressed as a step-wise shifting of the concentration values to the next discrete element with a step size dL/dt. As the flux of target molecules reaches the region of interest containing the antibody microarray, the binding reaction $C + B^e \rightarrow B^eC$ leads to concentration changes iteratively as follows:

$$d[BC] = (k_a[B^e][C] - k_d[BC])dt, \tag{1}$$

$$[C]_{T+dt} = [C]_T - d[BC], \tag{2}$$

$$[B]_{T+dt} = [B]_T - d[BC], \tag{3}$$

where k_a and k_d represent the forward and reverse reaction rates, respectively, dt represents the time segment to move the flux one unit length (dL) forward, and T the total time since the initiation of the reaction.

To identify a proper range within which the 1D-CR and 2D-FEM models would provide similar results of the captured targets $d[BC]$, we used the following parameters to perform a two-dimensional FEM (2D-FEM) simulation using COMSOL. The same parameters were used for all simulations, including the diffusion constant $D = 100\,\mu\text{m}^2/\text{s}$, flow rate $v = 450\,\mu\text{m/s}$, initial target concentration $C_0 = 10\,\text{nM}$, and estimated initial antibody surface density $B_0 = 6\,\text{nmol/m}^2$ (at 25% active binding sites) [39,40] with 1D-CR model fitted forward and reverse reaction constants $k_a = 7.60 \times 10^5\,\text{M}^{-1}\text{s}^{-1}$ and $k_d = 5 \times 10^{-4}\,\text{s}^{-1}$, respectively, which are consistent with the reported numbers in the literature.[41] The model geometry of the extended nanoslit was $700\,\mu$m long, with various slit heights, and a long microspot binding region of $500\,\mu$m was given to demonstrate the spatial distribution of the captured target molecules. The channel height was varied from $0.1\,\mu$m to $10\,\mu$m. The captured targets along the antibody microspots exhibited similar results when the slit heights were smaller than $1\,\mu$m but varied significantly as the slit height increased (Fig. 5(b)). The relative response was defined as the overall response from the 2D-FEM divided by the overall response from the 1D-CR model. As indicated in Fig. 5(c), slit heights less than $1\,\mu$m have a similar response ($\sim$100%), but the variation of the relative response increases as the slit height increases. Taking convection into account, we further used the Péclet number, Pe, as the ratio between the time required for diffusion and convection, which equals to $(H^2/2D)/(L/v)$. In the regime where $Pe < 1$ (our current experiment yields $Pe = 0.56$) the two models yield nearly identical results ($\sim$100%), showing that in the case of the extended nanochannel, the 1D-CR model describes the reaction kinetics with results similar to the 2D-FEM. As $Pe > 1$, the correlation decreases gradually where the assumption for 1D-CR model is no longer valid. To be noted, due to the spatial distribution of the captured target, which gives spatially distributed kinetic curves, one can determine kinetic constants with just one given target concentration, or to determine both unknown target concentration and surface probe density with known kinetic constants in a given experiment, a distinctive feature not found in other platforms, such as conventional QCM or SPR sensors.

CONCLUSIONS

This report presents the first real-time multiplex immunochemical reactions using antibody microarrays embedded in extended nanoslits. The technical challenge of the immobilization of multiplexed antibody spots in a miniaturized device was overcome with the help of a robotic microarrayer and the room-temperature-assisted PSQ bonding technique. We used fluorescently labeled antigens to reveal the binding kinetics in extended nanoslit devices. In a consecutive series of antibody spots, the upstream microspot exhibits a rapid onset of the fluorescence signal, and there is an inhomogeneity in fluorescence among the downstream microspots, indicating the high capturing efficiency of the antibody-antigen reaction resulting from confined slit heights. Experimentally obtained binding curves spatially distributed at multiple locations were combined and used for quantitative analysis on binding kinetics with a proposed 1D-CR model in a given experiment, specifically dedicated to reactions in extended nanoslits, where the diffusion is fast in comparison to convection and the reaction. The 1D-CR model provides consistent results with 2D-FEM data when $Pe < 1$ but with much improved simplicity and reduced computational resources. Hence our platform represents an integrated solution for real-time multiplexed immunosensing and kinetics monitoring, starting from device fabrication, protein immobilization, device bonding, sample transport, to data analysis. The fact that our platform is compatible with commonly available robotic microarrayer indicates the potential for low-cost expansion to large-scale multiplexing. Future prospects for this extended nanofluidic multiplexed immunoassay include experiments in which sample volumes are limited but sensing multiple biomarkers is required, such as with a finger-prick blood sample in clinical practice and single-cell analysis.

ACKNOWLEDGMENTS

We thank K.K. Sriram for helpful discussions and are grateful for technical support from the AS Nano Core Facilities. This work was supported by the AS Nano Program, AS Integrated Thematic Project (AS-103-TP-A01), Ministry of Science and Technology (MOST), Taiwan (102-2112-M-001-005-MY3 and 104-2119-M-001-011), the Asian Office for Aerospace Research and Development (FA2386-12-1-4002), and the Programme Blanc jointly sponsored by the Agence Nationale de la Recherche (ANR-13-IS10-0001) and MOST (103-2923-M-001-007-MY3).

[1]S. Vyawahare, A. D. Griffiths, and C. A. Merten, Chem. Biol. **17**, 1052 (2010).
[2]A. J. Tudos, G. A. J. Besselink, and R. B. M. Schasfoort, Lab Chip **1**, 83 (2001).
[3]J. Melin and S. R. Quake, Annu. Rev. Biophys. Biomol. Struct. **36**, 213 (2007).
[4]S. A. Mustafa, J. D. Hoheisel, and M. S. S. Alhamdani, Mol. BioSyst. **7**, 1795 (2011).
[5]Z. Kuang, J. J. Wilson, S. Luo, S.-W. Zhu, and R.-P. Huang, Int. J. Inflammation **2015**, 630637.
[6]S. Pelech, L. Jelinkova, A. Susor, H. Zhang, X. Q. Shi, A. Pavlok, M. Kubelka, and H. Kovarova, J. Proteome Res. **7**, 2860 (2008).
[7]A. Sandström, R. Andersson, R. Segersvärd, M. Löhr, C. A. K. Borrebaeck, and C. Wingren, Proteom. Clin. Appl. **6**, 486 (2012).
[8]R. Fan, O. Vermesh, A. Srivastava, B. K. H. Yen, L. Qin, H. Ahmad, G. A. Kwong, C.-C. Liu, J. Gould, L. Hood, and J. R. Heath, Nat. Biotechnol. **26**, 1373 (2008).
[9]R. B. Schoch, L. F. Cheow, and J. Han, Nano Lett. **7**, 3895 (2007).
[10]T. Leïchlé and C.-F. Chou, Biomicrofluidics **9**, 034103 (2015).
[11]R. Karnik, K. Castelino, R. Fan, P. Yang, and A. Majumdar, Nano Lett. **5**, 1638 (2005).
[12]K. Shirai, K. Mawatari, and T. Kitamori, Small **10**, 1514 (2014).
[13]R. P. Ekins and F. Chu, Trends Biotechnol. **12**, 89 (1994).
[14]C. Priest, Biomicrofluidics **4**, 032206 (2010).
[15]T. F. Didar, A. M. Foudeh, and M. Tabrizian, Anal. Chem. **84**, 1012 (2012).
[16]J. Gu, R. Gupta, C. F. Chou, Q. H. Wei, and F. Zenhausern, Lab Chip **7**, 1198 (2007).
[17]T. Leichle, Y. L. Lin, P. C. Chiang, S. M. Hu, K. T. Liao, and C. F. Chou, Sens. Actuator, B **161**, 805 (2012).
[18]R. Karnik, K. Castelino, C. Duan, and A. Majumdar, Nano Lett. **6**, 1735 (2006).
[19]W. Schrott, Z. Slouka, P. Cervenka, J. Ston, M. Nebyla, M. Pribyl, and D. Snita, Biomicrofluidics **3**, 44101 (2009).
[20]K. Mawatari, T. Tsukahara, Y. Sugii, and T. Kitamori, Nanoscale **2**, 1588 (2010).
[21]S.-Y. Seong, Clin. Diagn. Lab. Immunol. **9**, 927 (2002).
[22]F. Rusmini, Z. Y. Zhong, and J. Feijen, Biomacromolecules **8**, 1775 (2007).
[23]W. Kusnezow and J. D. Hoheisel, J. Mol. Recognit. **16**, 165 (2003).
[24]P. Angenendt, J. Glokler, D. Murphy, H. Lehrach, and D. J. Cahill, Anal. Biochem. **309**, 253 (2002).
[25]E. D. Dawson, A. E. Reppert, K. L. Rowlen, and L. R. Kuck, Anal. Biochem. **341**, 352 (2005).
[26]D. S. Rickman, C. J. Herbert, and L. P. Aggerbeck, Nucl. Acids Res. **31**, e109 (2003).
[27]J. Besecker, K. A. Cornell, and G. Hampikian, Sens. Actuators, B **176**, 118 (2013).
[28]X. J. Lou, N. J. Panaro, P. Wilding, P. Fortina, and L. J. Kricka, BioTechniques **36**, 248 (2004).
[29]H. Parsa, C. D. Chin, P. Mongkolwisetwara, B. W. Lee, J. J. Wang, and S. K. Sia, Lab Chip **8**, 2062 (2008).
[30]M. Zimmermann, E. Delamarche, M. Wolf, and P. Hunziker, Biomed. Microdevices **7**, 99 (2005).
[31]B. Goldstein, D. Coombs, X. He, A. R. Pineda, and C. Wofsy, J. Mol. Recognit. **12**, 293 (1999).
[32]A. Dodge, K. Fluri, E. Verpoorte, and N. F. de Rooij, Anal. Chem. **73**, 3400 (2001).
[33]Y. Gao, P. M. Sherman, Y. Sun, and D. Li, Anal. Chim. Acta **606**, 98 (2008).
[34]D. Kim and A. E. Herr, Biomicrofluidics **7**, 041501 (2013).
[35]P. E. Buckle, R. J. Davies, T. Kinning, D. Yeung, P. R. Edwards, D. Pollard-Knight, and C. R. Lowe, Biosens. Bioelectron. **8**, 355 (1993).
[36]T. M. Squires, R. J. Messinger, and S. R. Manalis, Nat. Biotechnol. **26**, 417 (2008).
[37]G. Q. Hu, Y. L. Gao, and D. Q. Li, Biosens. Bioelectron. **22**, 1403 (2007).
[38]E. Orabona, I. Rea, I. Rendina, and L. De Stefano, Sensors **11**, 9658 (2011).
[39]L. C. Shriver-Lake, B. Donner, R. Edelstein, B. Kristen, S. K. Bhatia, and F. S. Ligler, Biosens. Bioelectron. **12**, 1101 (1997).
[40]R. A. Williams and H. W. Blanch, Biosens. Bioelectron. **9**, 159 (1994).
[41]D. G. Myszka, J. Mol. Recognit. **12**, 390 (1999).